ADVANCED MATERIALS

attached crystals, and the morphology of the $CaCO_3$ was studied with scanning electron microscopy (Philips XL30FEG) after Au/Pd coating.

Received: September 9, 2002
Final version: January 9, 2003

[1] J. Aizenberg, A. Tkachenko, S. Weiner, L. Addadi, G. Hendler, *Nature* **2001**, *412*, 819.
[2] D. A. Bazylinski, *Chem. Geol.* **1996**, *132*, 191.
[3] S. Weiner, L. Addadi, *J. Mater. Chem.* **1997**, *7*, 689.
[4] N. Almqvist, N. H. Thomson, B. L. Smith, G. D. Stucky, D. E. Morse, P. K. Hansma, *Mater. Sci. Eng.* **1999**, *C7*, 37.
[5] S. Mann, B. R. Heywood, S. Rajam, J. D. Birchall, *Proc. R. Soc. London* **1989**, *A423*, 457.
[6] S. Mann, D. D. Archibald, J. M. Didymus, T. Douglas, B. R. Heywood, F. C. Meldrum, N. J. Reeves, *Science* **1993**, *261*, 1286.
[7] J. Aizenberg, A. J. Black, G. M. Whitesides, *J. Am. Chem. Soc.* **1999**, *121*, 4500.
[8] A. Berman, D. J. Ahn, A. Lio, M. Salmeron, A. Reichert, D. Charych, *Science* **1995**, *269*, 515.
[9] G. Falini, S. Albeck, S. Weiner, L. Addadi, *Science* **1996**, *271*, 67.
[10] A. L. Litvin, S. Valiyaveettil, D. L. Kaplan, S. Mann, *Adv. Mater.* **1997**, *9*, 124.
[11] J. Küther, G. Nelles, R. Seshadri, M. Schaub, H.-J. Butt, W. Tremel, *Chem. Eur. J.* **1998**, *4*, 1834.
[12] F. Lippmann, *Sedimentary Carbonate Minerals*, Springer-Verlag, Berlin **1973**, Ch. B.
[13] L. Wang, I. Sondi, E. Matijevic, *J. Colloid Interface Sci.* **1999**, *218*, 545.
[14] Joint Committee on Powder Diffraction Standards, Powder Diffraction File, Sets 1–5, Philadelphia, PA **1960**, Files 5-378, 5-417, 5-418.
[15] E. S. Dana, *Descriptive Mineralogy*, John Wiley & Sons, New York **1920**, Ch. VI.
[16] C. Park, R. E. Robertson, *J. Mater. Sci* **1998**, *33*, 3541.
[17] H. P. R. Frederikse, in *CRC Handbook of Chemistry and Physics* (Ed: D. R. Lide), CRC Press, Boca Raton, FL **2001**, Sec. 12.
[18] R. G. Larson, *The Structure and Rheology of Complex Fluids*, Oxford University Press, New York **1999**, Ch. 8.
[19] C. Y. Tai, F.-B. Chen, *AIChE J.* **1998**, *44*, 1790.
[20] J. Aizenberg, G. Lambert, S. Weiner, L. Addadi, *J. Am. Chem. Soc.* **2002**, *124*, 32.
[21] L. B. Gower, D. J. Odom, *J. Cryst. Growth* **2000**, *210*, 719.
[22] J. A. Speer, in *Reviews in Mineralogy*, Vol. 11 (Ed: R. J. Reeder), Mineralogical Society of America, Washington, DC **1983**, Ch. 5.
[23] E. I. Givargizov, *Oriented Crystallization on Amorphous Substrates*, Plenum Press, New York **1991**.
[24] V. R. Thalladi, G. M. Whitesides, *J. Am. Chem. Soc.* **2002**, *124*, 3520.
[25] C. A. Mitchell, L. Yu, M. D. Ward, *J. Am. Chem. Soc.* **2001**, *123*, 10830.

Face-Centered Cubic "Supracrystals" of Cobalt Nanocrystals**

By *Isabelle Lisiecki*, *Pierre-Antoine Albouy*, and *Marie-Paule Pileni**

Magnetic inorganic nanocrystals are being extensively studied because of the importance and wide range of their potential applications.[1–4] These include electronics, charge transport, and information storage, and require the synthesis of nanocrystals with well-defined sizes, shapes, and structures. Several challenges have to be faced. In particular, the organization of the nanoparticles on two-dimensional (2D) or 3D superlattices is important. These mesoscopic structures that bridge the gap between the microscopic atomic level and the macroscopic state can contribute to understanding magnetism in both regimes.

In the last three years, several groups have concentrated their efforts on producing self-organized magnetic nanocrystals in 2D networks. When magnetic nanocrystals are deposited on a surface, collective properties due to long-range dipolar interactions are observed.[5–15] Previously, we demonstrated that no change in the magnetic response is seen when the nanocrystals are organized in a 2D hexagonal network or short-range ordered.[16] Conversely, a marked change in the magnetic response is observed when the nanocrystals are aligned in a given direction.[16] This confirms previous data obtained in 3D assemblies of spherical[10,13] or cigar-like[15] maghemite nanocrystals aligned along a given direction by application of a magnetic field. This procedure presents serious drawbacks: it simultaneously induces a partial orientation of the easy axes[3] and an alignment of the nanocrystals without ordering on a 3D lattice.[10,14,15] These different effects change the magnetic response. The control of the self-organization of the nanocrystals in the absence of an external field is thus a key issue in understanding the relationship between structure (short-range or long-range order) and magnetic properties. Recently, "supracrystals" of non-magnetic nanoparticles (silver)[17–19] were made. Formation of such assemblies with magnetic nanocrystals was not expected because dipolar interactions prevent long-range organization.

In the present communication, it is demonstrated that face-centered-cubic (fcc) "supracrystals" can be produced using cobalt nanocrystals.

Cobalt nanoparticles coated with lauric acid were obtained as described in the Experimental section and dispersed in hexane after synthesis. Ten drops (10×10 μL) of a 3×10^{-7} M cobalt nanocrystal solution were deposited on an amorphous carbon-coated grid for transmission electron microscopy (TEM) examination. Figure 1A shows a very large coverage of nanocrystals. Their organization on a 2D hexagonal lattice is more clearly seen in the magnification in Figure 1B. This structure is further confirmed by the Fourier transform of this image as presented in Figure 1C. The estimated core diameter is 7.2 nm with 11 % size distribution and the interparticle gap is 2 nm (Fig. 1B). The length of the lauric acid molecule in the all-*trans* conformation is 1.77 nm[20] and corresponds to the maximum thickness of the particle coating. The experimentally found interparticle gap thus points to a dense lateral packing. High-resolution transmission electron microscopy (HRTEM) of a nanocrystal (inset in Fig. 1A) is sufficient to image the lattices and the pattern is consistent with multiple crystal orientations contained within a single nanocrystal. Samples obtained using a larger amount of deposited solution (20×10 μL) show the formation of multilayered "supracrys-

[*] Prof. M.-P. Pileni, Dr. I. Lisiecki
Laboratoire LM2N, UMR CNRS 7070
Université P. et M. Curie, Bât. F
4 Place Jussieu, F-75005 Paris (France)
E-mail: pileni@sri.jussieu.fr
Dr. P.-A. Albouy
Laboratoire de Physique des Solides, UMR 8502
Université Paris-Sud, Bât. 510
F-91405 Orsay (France)

[**] Thanks are due to Dr. A. T. Ngo from our laboratory for SEM images. We also thank D. A. Loiseau of ONERA (Châtillon) for providing us with facilities for using the transmission electron microscope.

  DOI: 10.1002/adma.200304417

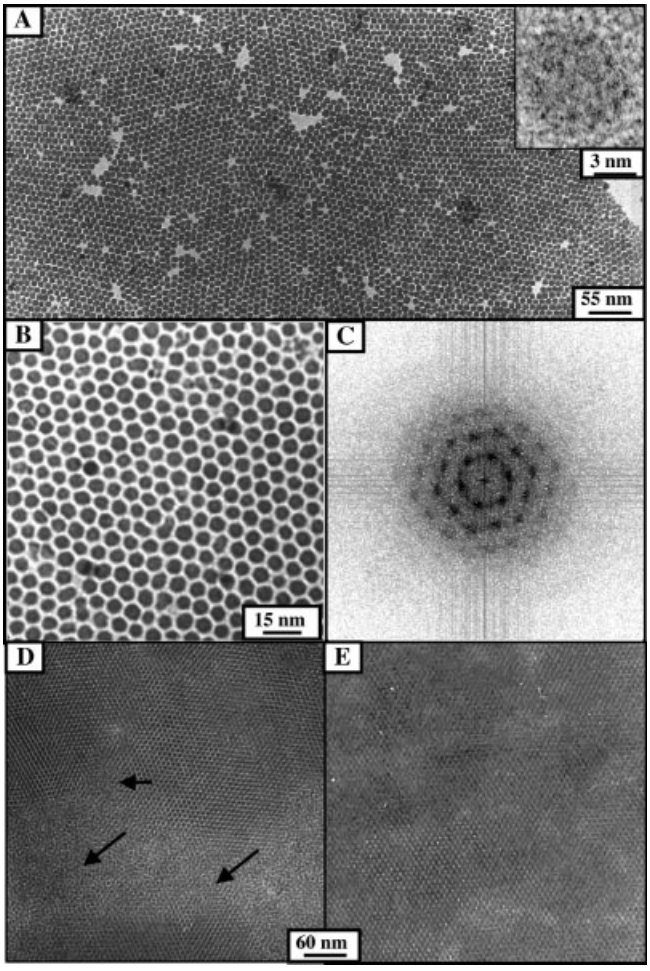

Fig. 1. A) TEM image of 7.2 nm cobalt nanocrystals organized in a compact hexagonal network. Inset: High-resolution pattern of a single cobalt particle. B) Selected area of (A). C) Fourier transform of (B). D) 3D superlattices obtained on amorphous carbon. E) 3D superlattices obtained on HOPG foils.

tals" as demonstrated in Figure 1D. However, defects in the organization are observed in some parts of the TEM grid (see arrows in Fig. 1D). Using highly oriented pyrolytic graphite (HOPG) as the substrate leads to a better organization of the nanoparticles (Fig. 1E). HOPG pieces (10 mm × 5 mm) were horizontally immersed in 200 μL of a highly concentrated nanocrystal solution (nanocrystal concentration 5.5×10^{-7} M) and the substrate temperature was kept at 25 °C by a Pelletier module. Solvent evaporation under a nitrogen atmosphere takes two hours.

Scanning electron microscopy (SEM; see Experimental section for details) was used to visualize the film morphology, which is found to consist of isolated grains separated by an average distance of 1.5 μm (Fig. 2A). The average height of the film was obtained by tilting the sample by 45° (Fig. 2B) and is about 5 μm. In addition, boundaries between grains display sharp edges. These broken edges, like the roughness of the film surface, are the result of surface tension stresses arising during evaporation. To verify the integrity of the magnetic particles, the grains were redispersed in hexane. A drop of the

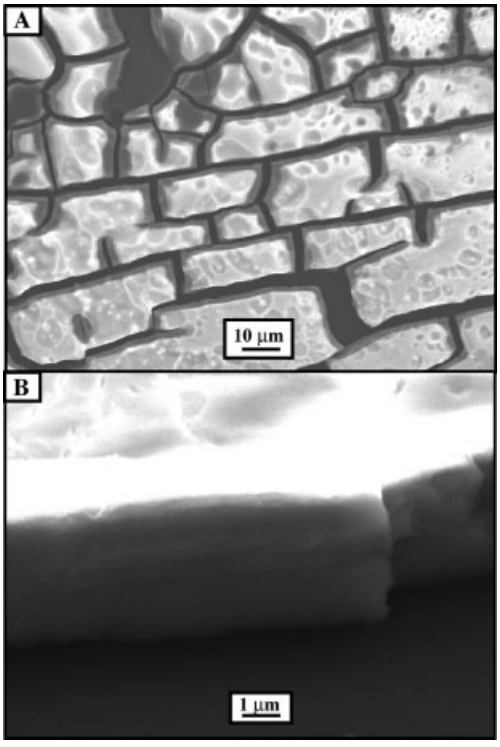

Fig. 2. SEM images of "supracrystals" at normal incidence (A) and at 45° tilt (B).

solution was deposited on a TEM grid and images similar to those shown in Figure 1 were observed.

To determine the local structure of these grains, small-angle X-ray diffraction (XRD) was performed. The small amount of scattering material dictates the choice of the specific instrumentation described in the Experimental section. Diffraction patterns were recorded on photo-stimulable imaging plates.[21] The XRD pattern (inset in Fig. 3) shows two reflections normal to the substrate. Figure 3 shows two well-defined Bragg reflections. The low intensity of the second order, and the absence of further diffraction orders, are due to the rapid decrease in the structure factor for spherical particles with increasing scattering angle (see below). The reflection width (Fig. 3) is nearly resolution-limited, indicating long-range or-

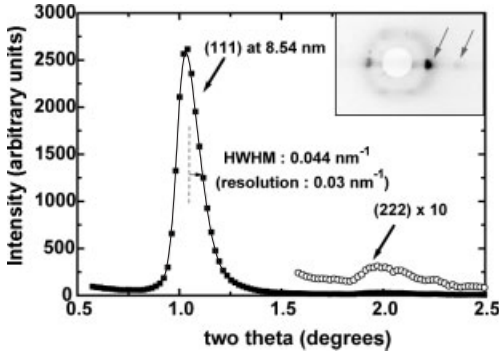

Fig. 3. Diffractogram of cobalt domains obtained by imaging plate scanning and corresponding to the X-ray diffraction pattern obtained in grazing incidence geometry (inset). (HWHM: half width at half maximum.)

ADVANCED MATERIALS

dering of the magnetic particles perpendicular to the surface. The stacking periodicity is 8.54 ± 0.05 nm. By rocking the sample around a vertical axis, it is qualitatively verified that the reflection range does not exceed a few tenths of a degree, which is the order of magnitude of the surface flatness for a HOPG substrate. It is proof of good alignment of the stacking planes with respect to the substrate. In order to increase the amount of irradiated material, the sample was tilted by ~10°. Figure 4 shows numerous additional diffraction spots with different intensities. For convenient visualization two different gray scales are used. It may be noticed that normal-to-the-

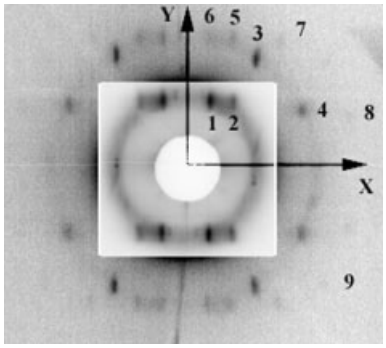

Fig. 4. X-ray diffraction pattern obtained in a nearly grazing incidence geometry (tilt angle of substrate surface with respect to the incoming beam: 10°); the intensity is reduced by a factor of 20 in the central inset.

plane reflections observed in Figure 3 are absent due to the sample tilt. These additional spots reveal a 3D long-range ordering within the nanocrystal domains. The observation of well-defined Bragg reflections in Figure 3 is proof that the ordered domains share a common crystallographic normal-to-the-substrate axis. It can be further assumed that their in-plane orientation is random.

The diffraction geometry is thus similar to that encountered in the oscillatory crystal method where Bragg reflections are brought into a reflection position by rotation around a crystallographic axis.[21]

A very similar situation may be found in ordered mesoporous films.[22,23] It can be reasonably assumed that the stacking planes parallel to the surface have a 2D hexagonal structure similar to that observed by TEM on single layers. Depending on the stacking sequence, fcc or hexagonal close-packed (hcp) structures are expected. The stacking periodicity $D\sqrt{2/3}$ is similar for both structures, where D is the coated particle diameter. The first-order reflection associated with this distance (Fig. 3) is indexed as (111) for fcc or (002) for hcp.[24] The experimental periodicity (8.54 nm) leads to a coated diameter D of 10.46 nm. This value includes the core diameter and a coating contribution. Using the core diameter value given by TEM leads to a coating contribution ~1.66 nm. This value is close to the all-*trans* length of lauric acid. A comparison of observed (Fig. 4) and calculated diffraction spot coordinates enables the two packings to be distinguished. In reciprocal space, (*hkl*) reflections are located on circles of radius q^y_{hkl} and elevation q^x_{hkl} with respect to the stacking direction. It is readily calculated that

$$q^y_{hkl} = \left(\frac{2\pi}{D}\right)\sqrt{\frac{(h^2+k^2+l^2\,hk-kl-hl)}{3}} \quad (1)$$

and

$$q^x_{hkl} = \left(\frac{2\pi}{D}\right)\left(\frac{h+k+l}{\sqrt{6}}\right) \quad (2)$$

for fcc packing, while

$$q^y_{hkl} = \left(\frac{2\pi}{D}\right)\sqrt{\frac{4(h^2+hk+k^2)}{3}} \quad (3)$$

and

$$q^x_{hkl} = \left(\frac{2\pi}{D}\right)\left(\frac{l}{\sqrt{3/8}}\right) \quad (4)$$

for hcp structures. In small-angle diffraction, the Ewald sphere may be considered as essentially planar. In these conditions, the x,y coordinates of the associated diffraction spots are, respectively, proportional to q^x_{hkl} and q^y_{hkl}. It is not possible to account for the experimental observations using a hcp structure. On the other hand, fcc packing leads to very satisfactory agreement between experimental and calculated data. The spot coordinates are reported in Table 1, where reciprocal distances have been converted into d-spacings using the well-known formula $q = 2\pi/d$ (the notation {h,k,l} here refers to a family of Bragg reflections located on the same reciprocal circle). The cubic parameter is $a = 14.79$ nm and is related to the diameter of the coated particle by $a = D\sqrt{2}$.

Table 1. Comparison between experimental and calculated coordinates of diffraction spots assuming a fcc structure; coordinates are expressed in d-spacings.

Reflection label (see Fig. 4)	{h,k,l} indices	x (meas.) [nm]	x (calc.) [nm]	y (meas.) [nm]	y (calc.) [nm]	d_{hkl} (meas.) [nm]	d_{hkl} (calc.) [nm]
1	1,1,–1	25.15	25.56	9.05	9.04	8.52	8.52
2	2,0,0	12.89	12.78	9.19	9.04	7.48	7.38
[a]	1,1,1	8.54	8.52	0	0	8.52	8.52
[a]	2,2,2	4.24	4.26	0	0	4.24	4.26
3	–1,3,1	8.53	8.52	5.24	5.22	4.46	4.45
4	1,1,3	5.12	5.11	9.51	9.04	4.51	4.45
5	2,2,–2	13.22	12.78	4.52	4.52	4.28	4.26
6	1,1,–3	26.09	25.56	4.47	4.52	4.41	4.45
7	4,0,0	6.38	6.39	4.55	4.52	3.70	3.69
8	3,3,1	3.67	3.65	10.10	9.04	3.45	3.39
9 [b]	4,2,0	4.31	4.26	5.44	5.22	3.38	3.30

[a] Not visible in Figure 3 due to the sample tilt angle; positions from Figure 4. [b] Reflection 9 is extremely weak.

The radius R of the cobalt core was further estimated by a qualitative comparison between measured and calculated intensities. For this, perfectly spherical cobalt spheres surrounded by a homogeneous organic medium were assumed. In that case, the structure factor is given by the well-known formula[25]

$$F(q) \propto \frac{(\sin qR - qR\cos qR)}{(qR)^3} \quad (5)$$

The intensity of diffraction spots of indices $\{h,k,l\}$ is thus

$$I_{hkl} \propto \frac{M_{hkl}}{q^{\gamma}_{hkl}} \left|F(q_{hkl})\right|^2 \quad (6)$$

where M_{hkl} is the multiplicity and $1/q^{\gamma}_{hkl}$ a Lorentz correction factor. No correction for absorption is introduced although the distance traveled by the diffracted beams through the sample is not negligible. The comparison between calculated and observed intensities is furthermore performed using only the most intense diffraction spots (Table 2). In view of the above mentioned approximations, a satisfactory agreement is obtained for $R \approx 3.54$ nm, very close to the TEM determination (3.6 nm). The experimental ratio of the first-order (111) and second-order (222) reflections is also close to the calculated value. This confirms that the coating thickness is close to 1.6 nm, as deduced above from the stacking periodicity. From these data it is concluded that the domains observed in Figure 2 are "supracrystals" of cobalt nanocrystals in a fcc structure.

Table 2. Comparison between experimental and calculated intensities for more intense diffraction spots (see Fig. 4); the ratio of the (111) and (222) Bragg reflections (Fig. 3) is also given. The particle radius used for the calculation is 3.54 nm.

Reflection label (see Fig.4)	$\{h,k,l\}$ indices	Intensity (meas.) [arbitrary units]	Intensity (calc.) [arbitrary units]
1	1,1,–1	1	1
2	2,0,0	0.48	0.54
3	–1,3,1	0.022	0.017
4	1,1,3	0.010	0.014
5	2,2,–2	0.004	0.012
6	1,1,–3	0.004	0.007
Intensity ratio (111)/(222):		143 (meas.)	171 (calc.)

The difference between the interparticle distance deduced from small-angle X-ray scattering (SAXS) on fcc "supracrystals" (3.2 nm) and data deduced from TEM on a monolayer in a compact hexagonal network (2 nm) is not easy to explain. However, tentative explanations can be proposed: i) The substrate used to grow "supracrystals" (HOPG) differs from that used to determine the interparticle distance (amorphous carbon). From previous data,[26,27] we know that the self-organization varies with the substrate. In the present case, for technical reasons, it was impossible to carry out the TEM experiments on HOPG. ii) We would also expect some relaxation of the interparticle distance when multilayers are formed.

In previous papers, "supracrystals" were made with silver nanocrystals coated with dodecanethiol.[19] It was demonstrated that, with time, the "supracrystals" degrade, with coalescence of silver particles. In the present work, cobalt nanocrystals coated with lauric acid remained stable; the "supracrystals" were kept for more than three months and the overall reflection spots remained present and at the same position. This is probably due to the greater strength of the coating with cobalt atoms compared to that with silver atoms.

The question arises why the dipolar interactions between cobalt nanocrystals do not prevent the growth of the "supracrystals". From the dipolar interactions modeled by Stoner and Wohlfarth for magnetic particles,[28,29] a coupling constant α_d is defined as

$$\alpha_d = \frac{\pi}{12} \frac{M_s^2}{K} (D/d)^3 \quad (7)$$

where K is the anisotropy constant (1.5×10^6 erg cm^{-3}), M_s the saturation magnetization (80 emu g^{-1}), D the magnetic particle diameter (7.2 nm), and d the center-to-center distance of the cobalt nanocrystals (10.46 nm). Superconducting quantum interference device (SQUID) measurements and diffraction data lead to an estimation of the coupling constant of 0.03. This rather low value could explain the formation of supracrystals.

In conclusion, "supracrystals" can be formed by slow evaporation of a solution of cobalt nanoparticles in hexane. The film consists of fcc single-crystal grains sharing a common crystallographic axis normal to the substrate and with an in-plane random orientation. These "supracrystals" remain stable with the same long-distance ordering for several months. This ability to form 3D ordered assemblies may be explained by the low value of the magnetic coupling constant. Now our new challenge is to be able to control the ordering of nanocrystals in these structures with the same coated cobalt nanocrystals.

Experimental

Synthesis: The synthesis of cobalt nanocrystals was carried out as described in previous papers [5,6]: reverse micelles of 5×10^{-2} M cobalt bis(2-ethylhexyl) sulfosuccinate, usually called $Co(AOT)_2$, form an isotropic phase. The amount of water added to the solution is fixed to give a water content, defined as $w = [H_2O]/[AOT]$, equal to 32. Sodium tetrahydroboride, $NaBH_4$, added to the micellar solution reduced the cobalt ions. Immediately after borohydride addition, the color of the micellar solution changed from pink to black, indicating the formation of colloidal particles. Addition of lauric acid, $C_{12}H_{25}COOH$, to the micellar solution induced a quasi-covalent attachment with cobalt atoms located at the interface. The coated cobalt nanocrystals were then extracted from reverse micelles by ethanol addition. The particles were subsequently washed and centrifuged several times with ethanol to remove all the surfactant. A black powder was obtained. The magnetic characteristics of the produced nanocrystals are similar to those of cobalt nanocrystals obtained previously and described in [5,6] with a saturation magnetization and a coercivity at 3 K of 80 emu g^{-1} and 0.10 T, respectively. This clearly indicates formation of cobalt nanocrystals. The nanocrystals were further dispersed in hexane.

Scanning Electron Microscopy: Scanning electron microscopy (SEM) was performed with a JMS-5510LV instrument. With the substrate tilted at an angle α for the scan, the height (H) of the aggregates was determined from $H = h/\sin\alpha$, where h is the height measured from the image and the scale bar is taken into account.

X-Ray Diffraction: X-ray experiments were performed with a rotating anode generator operated with a small-size focus (copper anode; focus size 0.2 mm × 0.2 mm; 50 kV, 30 mA). The optics consisted of a parabolic multilayer

ADVANCED MATERIALS

graded mirror followed by a bent nickel-coated mirror at right angles. It delivered a well-defined and intense parallel monochromatic beam. The sample was mounted on a rotation stage and the diffraction patterns were recorded on photo-stimulable imaging plates. Vacuum pipes were inserted between the sample and the image plate to reduce air scattering.

Received: September 9, 2002
Final version: December 12, 2002

[1] D. J. Sellmyer, M. Yu, R. D. Kirby, *Nanostruct. Mater.* **1999**, *12*, 1021.
[2] J. L. Dormann, D. Fiorani, E. Tronc, in *Advances in Chemical Physics*, Vol. 98 (Eds: I. Prigogine, S. A. Rice), Wiley, New York **1997**.
[3] J. Shi, S. Gider, K. Babcock, D. D. Awschalom, *Science* **1996**, *271*, 937.
[4] I. Billas, A. Châtelain, W. A. de Heer, *J. Magn. Magn. Mater.* **1997**, *168*, 64.
[5] C. Petit, A. Taleb, M.-P. Pileni, *J. Phys. Chem. B* **1999**, *103*, 1805.
[6] C. Petit, A. Taleb, M.-P. Pileni, *Adv. Mater.* **1998**, *10*, 259.
[7] C. B. Murray, S. Sun, W. Gaschler, H. Doyle, T. A. Betley, C. R. Kagan, *IBM J. Res. Dev.* **2001**, *45*, 47.
[8] S. Sun, C. B. Murray, D. Weller, L. Folks, A. Moser, *Science* **2000**, *287*, 1989.
[9] V. Russier, C. Petit, J. Legrand, M.-P. Pileni, *Phys. Rev. B* **2000**, *62*, 3910.
[10] T. Ngo, M.-P. Pileni, *Adv. Mater.* **2000**, *12*, 276.
[11] C. T. Black, C. B. Murray, R. L. Sandstrom, S. Sun, *Science* **2000**, *290*, 1131.
[12] V. Russier, *J. Appl. Phys.* **2001**, *89*, 1287.
[13] T. Ngo, M.-P. Pileni, *J. Phys. Chem.* **2001**, *105*, 53.
[14] J. Legrand, C. Petit, M.-P. Pileni, *J. Phys. Chem. B* **2001**, *105*, 5643.
[15] T. Ngo, M.-P. Pileni, *J. Appl. Phys.* **2002**, *92*, 4649.
[16] C. Petit, V. Russier, M.-P. Pileni, unpublished.
[17] L. Motte, F. Billoudet, M.-P. Pileni, *J. Phys. Chem.* **1995**, *99*, 16 425.
[18] C. B. Murray, C. R. Kagan, M. Bawendi, *Science* **1995**, *270*, 1335.
[19] A. Courty, C. Fermon, M.-P. Pileni, *Adv. Mater.* **2001**, *13*, 254.
[20] C. D. Bain, E. B. Troughton, Y. T. Tao, J. Evall, G. M. Whitesides, R. G. Nuzzo, *J. Am. Chem. Soc.* **1989**, *111*, 321.
[21] See, e.g., B. E. Warren, *X-Ray Diffraction*, Dover Publications, New York **1990**, p. 85.
[22] M. Klotz, P. A. Albouy, A. Ayral, C. Ménager, D. Grosso, A. Van der Lee, V. Cabuil, F. Babonneau, C. Guizard, *Chem. Mater.* **2000**, *12*, 1721.
[23] D. Grosso, A. R. Balkenende, P. A. Albouy, M. Lavergne, L. Mazerolles, F. Babonneau, *J. Mater. Chem.* **2000**, *10*, 2085.
[24] See, e.g., Y. Sakamoto, I. Díaz, O. Terasaki, D. Zhao, J. Pérez-Pariente, J. M. Kim, G. D. Stucky, *J. Phys. Chem. B* **2002**, *106*, 3118.
[25] A. Guinier, *X-Ray Diffraction in Crystals, Imperfect Crystals, and Amorphous Bodies*, Dover Publications, New York **1994**, p. 323.
[26] A. Courty, M.-P. Pileni, unpublished.
[27] L. Motte, E. Lacaze, M. Maillard, M.-P. Pileni, *Langmuir* **2000**, *16*, 3803.
[28] C. Stoner, E. P. Wohlfarth, *Philos. Trans. R. Soc. London A* **1948**, *240*, 599; reprinted in *IEEE Trans. Magn.* **1991**, *27*, 3475.
[29] H. Pfeiffer, *Phys. Status Solidi A* **1990**, *122*, 377.

A Strong Correlation Between the Hole Mobility and Silicon Chain Length in Oligosilane Self-Organized Thin Films

By *Hajime Okumoto*,* *Tetsuo Yatabe*, *Andrew Richter*, *Junbiao Peng*, *Masaki Shimomura*, *Akira Kaito*, and *Nobutsugu Minami*

Organic molecular electronics is an intensively studied field, producing various types of functionality and devices such as photoconductors, electroluminescent devices, and field-effect transistors. While many of these studies are focused on π-conjugated materials, σ-conjugated materials[1] have emerged as promising organic carrier transport materials. Polysilanes, possessing σ-conjugated electrons delocalized along Si main chains, have been extensively investigated because of their relatively high hole mobility on the order of 10^{-4} $cm^2 V^{-1} s^{-1}$ at room temperature.[2,3] The hole transport, however, is characterized by structural disorder[3,4] due to the inevitable distribution of the molecular weight of polymers and their random orientation.

We have been working on oligosilanes as a new type of carrier transport material because they can be monodispersed and they possess a remarkable self-organizing property. We expect that the self-organization of molecules is a key factor to strategically control various functions of organic electronic materials on the basis of the high molecular order. Indeed, some oligosilanes are known to have a smectic B (S_B) phase, which is a mesophase between an isotropic phase and a crystalline (C) phase.[5–7] Moreover, we found that the multilayer structure in the S_B phase is mostly preserved in the polycrystalline phase, where molecules are oriented normal to the substrate with a large domain size (> 20 μm).[8]

We have already studied the carrier transport properties of decasilane thin films in connection with their self-organized structures.[8,9] Because of the high molecular order and the large domain size, they demonstrate excellent transport properties, as shown by non-dispersive time-of-flight (TOF) transient photocurrent waveforms with a clear plateau and a sharp decay. The textbook-like waveforms indicate a narrow distribution of the hole mobility and the minimal effects of traps. The molecular orientation normal to the substrate, parallel to the applied electric field, results in high hole mobility, achieving a value of 1.3×10^{-3} $cm^2 V^{-1} s^{-1}$ for polycrystalline thin films of permethyldecasilane $CH_3[Si(CH_3)_2]_{10}CH_3$ (MS10) at room temperature. Moreover, the transport properties are qualitatively different from those of the disordered materials. For example, the mobility, μ, depends on the electric field E as $\log \mu \propto E$. This is markedly different from $\log \mu \propto \sqrt{E}$ as is usually observed for disordered materials, including polysilanes.[3,4,10,11]

In the present work, we investigated the effects of molecular length on the transport properties of self-organized oligosilane polycrystalline thin films. A series of permethyloligosilanes with different lengths $CH_3[Si(CH_3)_2]_nCH_3$ (MSn, n = 8–12) were used, whose schematic structures are shown in Figure 1a. We have found strong correlations among the molecular length, the self-organized structure, and the carrier transport properties. Of particular interest is an *odd–even* effect in the hole mobility with respect to the number of Si repeat units. We stress that such an effect should only occur for ordered systems with exceptionally long correlation lengths.

A series of permethyloligosilanes MS8–MS12 were synthesized and purified following a previous method.[5] It is known that MS9–MS12 show the S_B phase between the crystalline and isotropic phases, while MS8 does not. For photocurrent measurements, powder of each oligosilane was melted and capillary-filled into a gap (~10 μm) between two quartz sub-

[*] Dr. H. Okumoto, Dr. T. Yatabe, Dr. A. Richter, Dr. J. Peng, Dr. M. Shimomura, Dr. A. Kaito, Dr. N. Minami
Nanotechnology Research Institute
National Institute of Advanced Industrial Science and Technology (AIST)
Tsukuba, Ibaraki 305–8565 (Japan)
E-mail: okumoto-h@aist.go.jp

  DOI: 10.1002/adma.200304809